

Cosmic ray feedback in galaxies and active galactic nuclei

C. Pfrommer^{1,a)}, R. Pakmor¹, K. Schaal^{1,2}, C. M. Simpson¹ and V. Springel^{1,2}

¹*Heidelberger Institut für Theoretische Studien, Schloss-Wolfsbrunnenweg 35, 69118 Heidelberg, Germany*

²*Zentrum für Astronomie der Universität Heidelberg, Astronomisches Recheninstitut, Mönchhofstr. 12-14, 69120 Heidelberg, Germany*

^{a)}Corresponding author: christoph.pfrommer@h-its.org

Abstract. Recent cosmological simulations of galaxy formation have demonstrated that feedback by star formation, supernovae and active galactic nuclei appears to be critical in obtaining realistic disk galaxies, to slow down star formation to the small observed rates, to move gas and metals out of galaxies, and to balance radiative cooling of low-entropy gas at the centers of galaxy clusters. However the particular physical processes underlying these feedback processes still remain elusive. In particular, these simulations neglected cosmic rays (CRs) and magnetic fields, which provide a comparable pressure support in comparison to turbulence in our Galaxy, and are known to couple dynamically and thermally to the gas. We will present our recent efforts to model CR physics in the cosmological simulation code AREPO and demonstrate that CRs matter on all scales relevant for galaxy formation. Presenting global simulations of galaxy formation that couple CRs to the magneto-hydrodynamics, we show how CRs can launch powerful galactic winds, which reduces the available amount of gas for star formation. In particular, we highlight the importance of the γ -ray window in understanding the properties of galactic winds and discuss the non-thermal radio and γ -ray emission of Milky-Way like galaxies with bubble-shaped outflows. On scales of galaxy clusters, we show that cosmic-ray heating can balance radiative cooling of the low-entropy gas at the centers of galaxy clusters and helps in mitigating the star formation of the brightest cluster galaxies. Combining low-frequency radio and γ -ray emission of M87, the closest active galaxy interacting with the cooling cluster plasma, enable us to put forward a comprehensive, physics-based model of feedback by active galactic nuclei.

INTRODUCTION AND MOTIVATION

Understanding the physics of galaxy formation is arguably one of the most interesting problems in modern astrophysics. According to our current cosmological standard model, galaxies form in (slowly rotating) dark matter halos [1]. Since the radiative cooling time of the gas is shorter than the age of the galaxies [2], the gas cools and diminishes its pressure support in the center. As a result it collapses while conserving its specific angular momentum, thus settling into a rotationally supported cold disk. In the disk, the gas is compressed by self-gravity to sufficiently high densities that star formation ensues. In the absence of any feedback process we would expect all baryonic gas to be converted to stars. However, applying abundance matching arguments shows that at most 20% of the available gas is transformed to stars at the scale of the Milky Way and that the star conversion efficiency plummets towards smaller and larger mass scales [3].

A large body of theoretical work based on cosmological simulations and semi-analytic models has demonstrated that feedback processes by stellar winds and radiation fields, supernovae, and active galactic nuclei (AGNs) appear to be critical in obtaining realistic galaxy populations [4, 5, 6, 7, 8, 9, 10, 11]. These processes are invoked to slow down star formation to the small observed rates, to transfer gas and metals from galaxies into the intergalactic medium by means of galactic winds, to obtain a realistic mix of early- and late-type galaxies, to quench star formation in elliptical galaxies, and to balance radiative cooling of low-entropy gas at the centers of galaxy clusters so that global cluster observables agree with observations in the X-ray regime.

While the recent progress of galaxy formation models is remarkable, it still comes with the caveat that the involved feedback has typically been modeled empirically and tuned to match observed galaxy scaling relations, weakening the predictive power of the corresponding calculations. In particular, feedback in hydrodynamical simulations of galaxy formation has thus far often been implemented very coarsely, for example based on explicit subgrid models that aim to represent the unresolved, multi-phase structure of the interstellar medium (ISM) with an effective descrip-

tion that still yields the correct average star formation rate [12, 13]. The physics behind galactic winds and outflows remains especially unclear, and is sometimes treated in a purely phenomenological way where the wind velocity and momentum flux are prescribed [14]. Similarly, in order to prevent too many stars from precipitating out of the hot phase of the intra-cluster medium (ICM), feedback from AGN has often been modeled by estimating accretion rates with a simple Bondi prescription and injecting thermal energy as feedback [15, 16].

What are the physical mechanisms responsible for launching galactic winds? There are three major processes proposed, including (1) thermal pressure provided by supernovae or AGNs, (2) radiation pressure and photoionization by massive stars and quasars, and (3) CR pressure and Alfvén-wave heating of CRs accelerated at supernova shocks. It has proven to be challenging to launch powerful winds with substantial mass-loading factors by thermal pressure of the hot gas that was generated by repeated supernovae [17, 18]. This is because thermal energy deposited in the dense phase is quickly radiated away or – provided the collective action of stellar winds and supernovae is sufficiently strong – drives hot chimneys and superbubbles that start to launch galactic outflows [19], which however show a low mass loading factor. It was proposed that momentum-driven winds could result from radiation pressure acting on dust grains and atomic lines in dense gas, imparting enough momentum to accelerate the gas, potentially explaining strong outflows in starburst galaxies [20, 21]. However, direct radiation-hydrodynamics simulations of the Rayleigh-Taylor instability [22] and large-scale galaxy models [23, 24] fail to see strong, mass-loaded winds because the radiation is not sufficiently trapped (as assumed in more simplified analytical calculations) but instead also generates a channel structure along which a substantial fraction of the radiation is able to escape.

On the other hand, CRs and magnetic fields are observed to be in pressure equilibrium with the turbulence in the midplane of the Milky Way [25]. This could be naturally explained if it is the outcome of a self-regulated feedback loop where CRs provide the main wind driving mechanism, as suggested by a number of theoretical works [26, 27, 28, 29, 30, 31, 32, 33, 34, 35] and local three-dimensional simulations of the ISM [36, 37, 38]. In fact, there are a number of arguments that point to this possibility. (1) Polarized radio observations of edge-on galaxies show poloidal field lines at the disk-halo interface [39]. This argues for a dynamical mechanism that is responsible for reorienting the toroidal magnetic field in the disk and may be explained by a CR-driven Parker instability [40]. (2) The CR pressure drops less quickly than thermal pressure upon adiabatic expansion from the disk ($P \propto \rho^\gamma$) due to its softer relativistic equation of state. (3) CRs cool less efficiently than thermal gas, which enables storing their energy for a longer time. (4) CR pressure energizes the wind by means of Alfvén wave heating, which justifies the analogy of a ‘CR battery’ that is transported alongside and releases energy on a longer time, thereby modifying the thermal structure of such a wind. Indeed, recent hydrodynamical simulations of the formation and evolution of disk galaxies have shown that CR pressure can drive strong bipolar outflows in disk galaxies provided CRs are allowed to stream [41, 42] or diffuse [43, 44, 45] relative to the rest frame of the gas.

In addition, CRs may hold the key to understanding a similar problem in giant elliptical galaxies located at the centers of galaxy groups and clusters. A net outward flux of streaming CRs may provide a means to stably heat the cooling cluster plasma by the excitation of resonant Alfvén waves. Once generated, they experience non-linear Landau damping or decay via a cascading process as a result of strong external turbulence, and eventually dissipate locally [46, 47, 48, 49, 50, 51, 52, 53]. These considerations provide motivation for pursuing a study that employs modern hydrodynamical cosmological simulation codes with a numerically efficient and accurate treatment of CR physics coupled to magneto-hydrodynamics (MHD), the first result of which will be presented here. After reviewing the characteristics of CR transport and our modeling approach, we demonstrate how the γ -ray window can be used in constraining CR feedback in galactic outflows and active galactic nuclei.

MODELING COSMIC RAY PHYSICS IN GALAXY FORMATION

We model the physics of galaxy formation with the cosmological hydrodynamic code `AREPO`. It solves the coupled system of hyperbolic conservation laws by discretizing the hydrodynamic quantities on a moving unstructured mesh defined by the Voronoi tessellation of a set of discrete points [54]. We calculate the fluxes of conserved variables across the moving interface from the reconstructed primitive variables using an approximate Riemann solver as previously described [55].

A simplified overview over the relevant physical processes in galaxy formation that we model in `AREPO` is given in Fig. 1. The *upper central part* shows standard processes which are usually considered in simulations. Radiative cooling of the gas leads eventually to star formation in the densest regions of the ISM that exceed a certain density threshold. Once the nuclear energy of stars has been used up, stars more massive than eight solar masses explode as core-collapse supernovae that drive strong shocks into the ambient ISM which resupply thermal and turbulent energy.

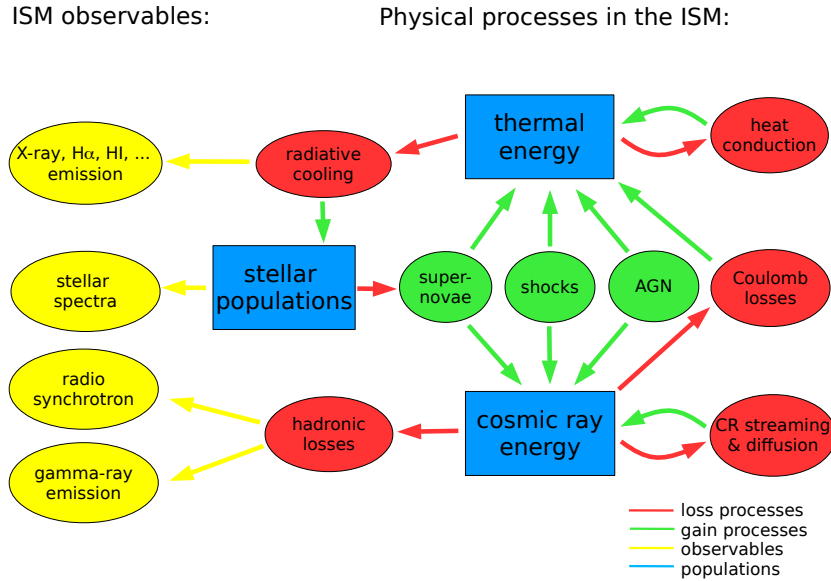


FIGURE 1. Overview over the relevant physical processes in galaxy formation. The center and right-hand side shows the interplay of different physical processes while the left-hand side shows observables that inform about the properties of galaxies. Gain processes are denoted in green and loss respectively redistribution processes are denoted in red.

In the center of galaxies, the AGN can energize the ambient medium in form of a quasar wind or transport momentum to larger scales by means of a relativistic jet. On even larger scales, structure formation shocks dissipate gravitational energy associated with hierarchical clustering into thermal energy of the gas, thus supplying the intergalactic medium with entropy and thermal pressure support. There are a number of observables associated with the cooling processes: the hot phase of the ISM emits thermal bremsstrahlung and line radiation up to X-ray energies, H- α emission traces the warm ionized phase, while H I and molecular emission indicates the cold phase harboring star formation.

The *lower part* of Fig. 1 sketches the CR physics relevant to the formation and evolution of galaxies. CRs behave differently compared to the thermal gas. Their equation of state is softer, they are able to travel actively over macroscopic distances, and their energy loss time-scales are typically larger than the thermal ones. Besides thermalization, collisionless shocks are also able to accelerate ions of the Maxwellian through diffusive shock acceleration [for a review see 56], which typically yields a CR population with a power-law distribution of the particle momenta. CRs are accelerated through supernova shocks in the ISM, in AGN jets, and at structure formation shock waves on larger scales in the intergalactic medium. Using an on-the-fly shock finder, we characterize shocks in our simulations and inject CRs at resolved shocks in the computational domain [57], at AGN jets, and at supernova remnants that are individually not resolved in simulations of galaxy formation, but that follow star formation and feedback in a sub-resolution framework.

So far, our approach follows the advective transport of CRs with the magnetized plasma as well as the anisotropic diffusive transport along the local magnetic field lines. For the latter, we employ a gradient-limited, conservative, semi-implicit scheme for anisotropic CR diffusion that supports local time stepping [58]. We account for the most important CR loss processes in the form of Coulomb and hadronic interactions with the thermal plasma by adopting an equilibrium CR distribution that results from a balance between injection and dissipation processes [57]. Furthermore, we also model CR energy losses as a result of the generation of Alfvén waves by the CR streaming instability [59]. On the lower left of Fig. 1, we show the main CR observables that are generated as CR protons interact inelastically with nuclei of the ambient thermal gas and produce pions, which decay into γ rays, secondary electrons/positrons, and neutrinos. The combination of observables associated with pion-decay γ rays, the secondary radio synchrotron and inverse Compton (IC) γ -ray emission enables to infer properties about the CR transport processes. This novel element enables us to study problems associated with CR acceleration at supernova remnants, and to understand the dynamical impact of CRs on galaxy formation and the evolution of galaxy clusters.

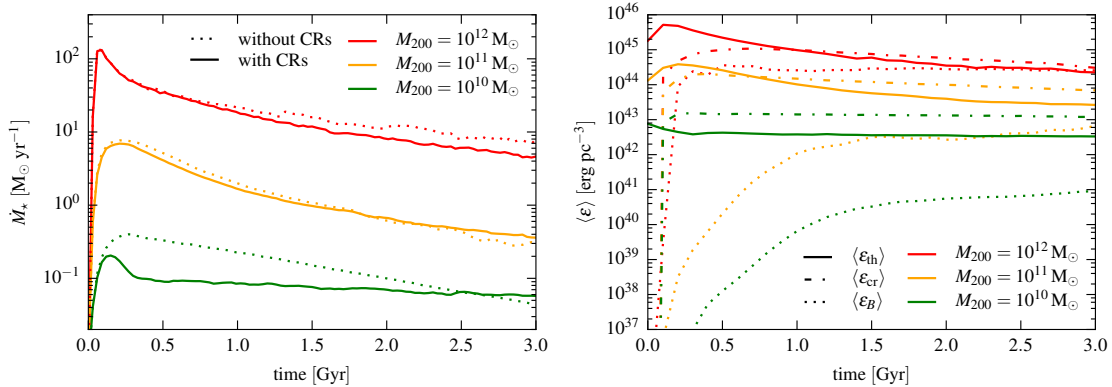


FIGURE 2. Time evolution of the star formation rate (left panel) and the average energy densities in a disk of radius 10 kpc and height 1 kpc that is centered on the mid-plane (right panel). Different halo masses with 10^{10} , 10^{11} , and $10^{12} M_\odot$ are color coded. Simulations with advective CR feedback (solid lines) suppress star formation more strongly in smaller galaxies in comparison to simulations without CRs (dotted lines). The right panel shows the evolution of the thermal energy density, CR energy density, and magnetic energy density, respectively, in our MHD simulations which account for CR acceleration at supernova remnants and follow advective transport (adapted from [57]).

COSMIC RAY FEEDBACK IN GALAXY FORMATION

To explore the impact of CR physics on MHD simulations of galaxy formation, we run a set of MHD simulations that follow the formation of galaxies in isolation and vary the complexity of the CR transport. We start with purely advective CR transport and then additionally account for (an-)isotropic CR diffusion. Starting from a slowly rotating NFW dark matter halo that is filled with gas and tiny seed magnetic fields, the onset of radiative cooling causes the formation of a central galactic disk from the inside out. First, we model CR injection at supernovae, advective CR transport, and Coulomb and hadronic CR interactions with the ambient gas (for details, see [57]). We find that CR pressure feedback suppresses star formation more strongly in smaller galaxies in comparison to simulations without CRs (see Fig. 2). During the first starburst, the CR energy density in the disk quickly reaches equilibrium with the thermal energy density and dominates the internal energy budget soon thereafter. The slowly cooling non-thermal pressure reservoir provided by CRs causes the disks to be more expanded in the vertical direction, providing additional dynamical stability to a disk that would otherwise be unstable to gravitational collapse (see Fig. 3).

The local injection of CR energy at supernovae modifies the multi-phase structure of the ISM, which exhibits an amorphous clumpy structure when CR physics is included. Without CRs, this multiphase structure is mostly suppressed by the stiff effective equation of state above of the adopted subgrid model for star formation and its regulation (cf. panels (a) and (b) of Fig. 3). We envision that such a multiphase structure as a result of local CR feedback will also be maintained when we additionally account for CR streaming and diffusion, and employ a temporarily and spatially varying diffusion coefficient. The latter is expected to increase with distance from the location of supernova remnants and reach the average Galactic value on large scales.

Initially, all our galaxy models with halo masses ranging from 10^{10} to $10^{12} M_\odot$ exhibit a rapid turbulent dynamo for the magnetic field that eventually transitions to a slower amplification process (right panel of Fig. 2). This also increases the magnetic coherence scale as the field is wound up by differential rotation of the disk. The field structure is very regular and quiet in the simulations without CRs, reflecting the pressurized equation of state of the ISM. In contrast, in our CR simulations, it attains a chaotic small-scale component which is superimposed on the dominant azimuthal structure. We find that the additional turbulent velocity field is a result of supernova explosions that sustain an additional dynamo action, amplifying the field to observed strengths exceeding $10 \mu\text{G}$ in the centers of the disks.

The ability of CRs to drive winds is intimately tied to their active transport processes relative to the gas rest frame. In particular, the fast streaming of CRs along the magnetic field excites Alfvén waves through the streaming instability [59]. Scattering off of this wave field limits the CRs’ bulk speed in turn. These waves are then damped, effectively transferring CR energy and momentum to the thermal plasma. Hence CRs exert a pressure on the thermal plasma by means of scattering off of Alfvén waves. In addition, CRs are diffusing in the Alfvén frame.

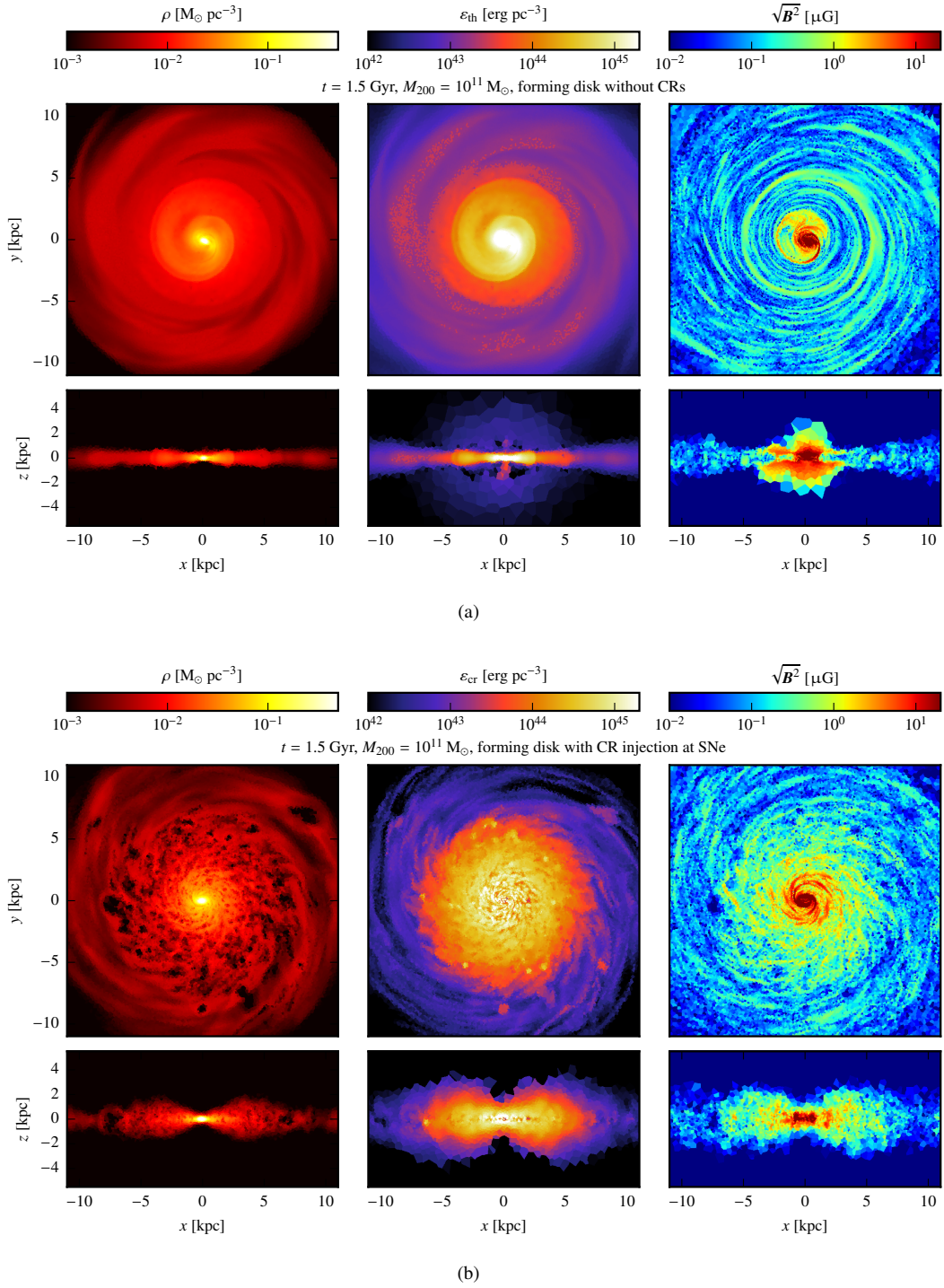


FIGURE 3. Properties of the gas disk in our $10^{11} M_{\odot}$ halo after 1.5 Gyr in MHD simulations without CRs (a) and where we inject CRs with our supernova remnant model and follow their advection with the gas (b). We show cross-sections of gas properties in the mid-plane of the disk as face-on views and vertical cut-planes through the center as edge-on views of the gas density (left panels), CR and thermal energy density (middle panels, (a) and (b), respectively), and the magnetic field strength (right panels, adapted from [57]).

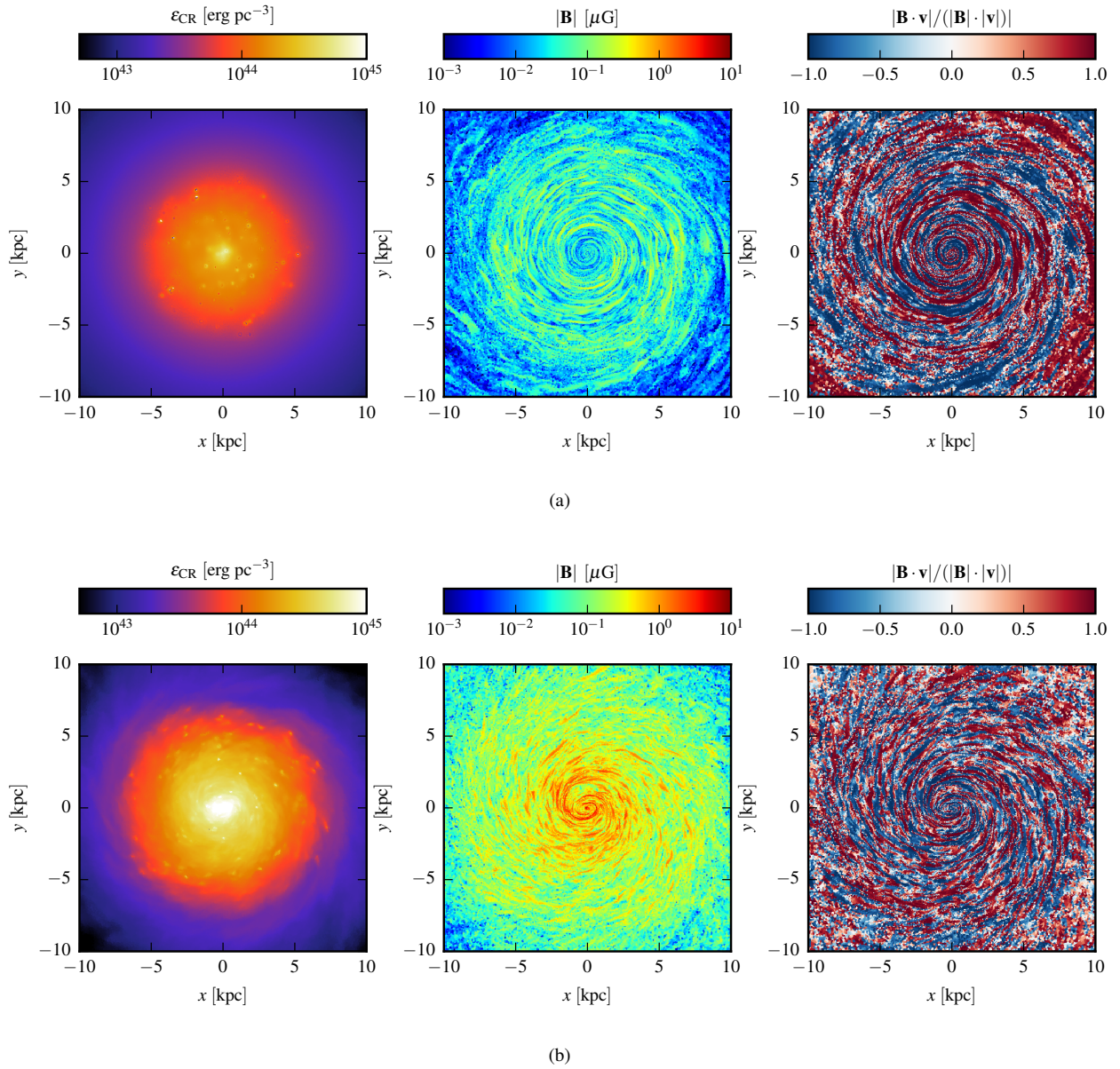


FIGURE 4. Properties of the gas disk in our $10^{11} M_{\odot}$ halo after 1.5 Gyrs for the runs with isotropic CR diffusion (a) and anisotropic CR diffusion (b). The columns show slices in the midplane of the disk. From left to right, the color-coded maps show the CR energy density, the magnetic field strength, and the cosine of the angle between the directions of the magnetic field and the velocity field (adapted from [60]).

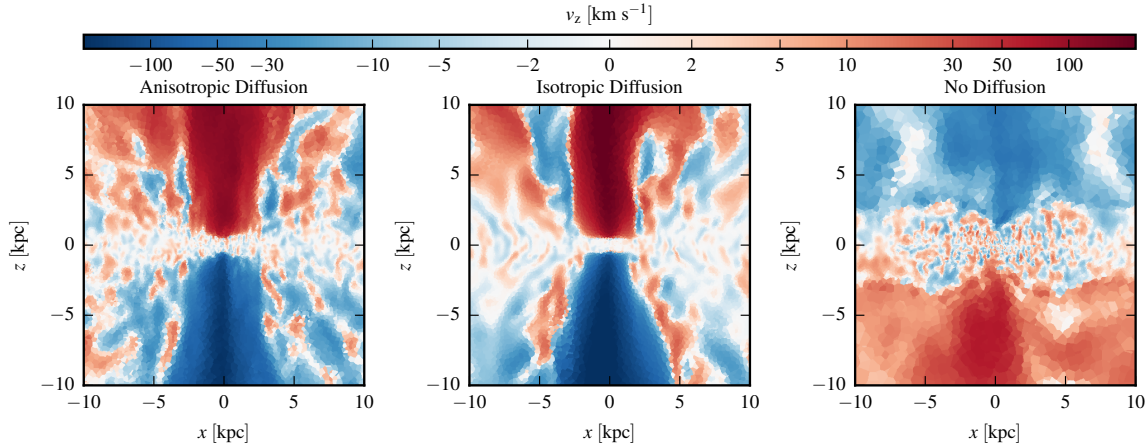


FIGURE 5. Slices in the $x - z$ plane through the center of the disk in our $10^{11} M_{\odot}$ halo, showing the z -velocity component after 1.5 Gyrs. The columns from left to right correspond to the simulations with anisotropic CR diffusion, isotropic CR diffusion, and without CR diffusion, respectively (adapted from [60]).

In our simulations with isotropic diffusion, we assume a constant diffusion coefficient of $10^{28} \text{cm}^2 \text{s}^{-1}$. For anisotropic diffusion, we adopt the same value parallel to the magnetic field and no diffusion perpendicular to it (for details see [60]). After 1.5 Gyrs, the gas densities in the disks are very similar in the simulations with isotropic and anisotropic CR diffusion. They strongly peak in the center, where most of the stars are formed and thus most of the CRs are injected. In the isotropic diffusion model, CRs are then isotropically transported outwards and settle into an almost spherical distribution. In contrast, with anisotropic diffusion, CRs can only be transported along magnetic field lines and therefore the diffusion process is very sensitive to the structure of the magnetic field (see Fig. 4).

The magnetic field strength is initially (in the first 300 Myrs) amplified exponentially on very small scales to a field strength of about $10^{-2} \mu\text{G}$, consistent with a turbulent small-scale dynamo and showing little dependence on whether we account for diffusion or not. After this initial phase the disk has formed and the differential rotation in the disk dominates the velocity field. The magnetic field continues to grow exponentially, but on much longer timescales, indicating that the dominant amplification mechanism has changed. Around that time, the structure of the magnetic field also changes from a chaotic small-scale field to one completely dominated by its toroidal (i.e., azimuthal disk) component. Note that even though the magnetic field is essentially completely aligned with the velocity field, it features a large number of field reversals (right panels of Fig. 4).

For the simulation with anisotropic diffusion, this magnetic field structure implies that within the first 300 Myrs, the CRs diffuse essentially isotropically, but with a significantly lower effective diffusion coefficient as they are not transported along straight lines on large scales but are forced to random walk. At later times, however, they are mostly trapped at their radial and vertical positions and are only transported along the angular coordinate. Thus, a much larger fraction of the injected CRs remains in the disk as compared to the run with isotropic diffusion. Perhaps the strongest indication of a difference in the dynamic state of the ISM for the different types of diffusion can be seen in the strength of the magnetic field. After 1.5 Gyrs, the typical magnetic field strength in the anisotropic diffusion run is about $1 \mu\text{G}$. In contrast, in the isotropic diffusion run it only reaches a field strength of order $0.1 \mu\text{G}$ by this time. Since the structure of the magnetic field is very similar in both runs, it appears that either the same amplification mechanism works with different efficiencies in the two runs, or that different amplification mechanisms dominate in the two runs.

Most importantly, the different modes of CR transportation result in dramatic differences in their dynamical effect on the gas. As shown in Fig. 5, both simulations with diffusion develop strong centralized bipolar outflows. After 1.5 Gyrs, the outflows have mass loading factors of 1.0 (measured at a height of 5 kpc above and below the disk and within a radius of 10 kpc) and 1.1 in the runs with anisotropic diffusion and isotropic diffusion, respectively. In contrast, the run without diffusion does not develop any large scale outflows. Instead, it shows a strong fountain flow up to a height of 2-3 kpc. This fountain flow is also present in the diffusion runs, but is suppressed in the simulation with isotropic diffusion. In this calculation, the vertical velocity field in the disk (excluding the bipolar outflow) seems to be generally lower and lacks small-scale structure. Note that in both diffusion runs we additionally see what looks like a large-scale fountain flow over the disk, outside the central outflow, that reaches beyond 10 kpc in height.

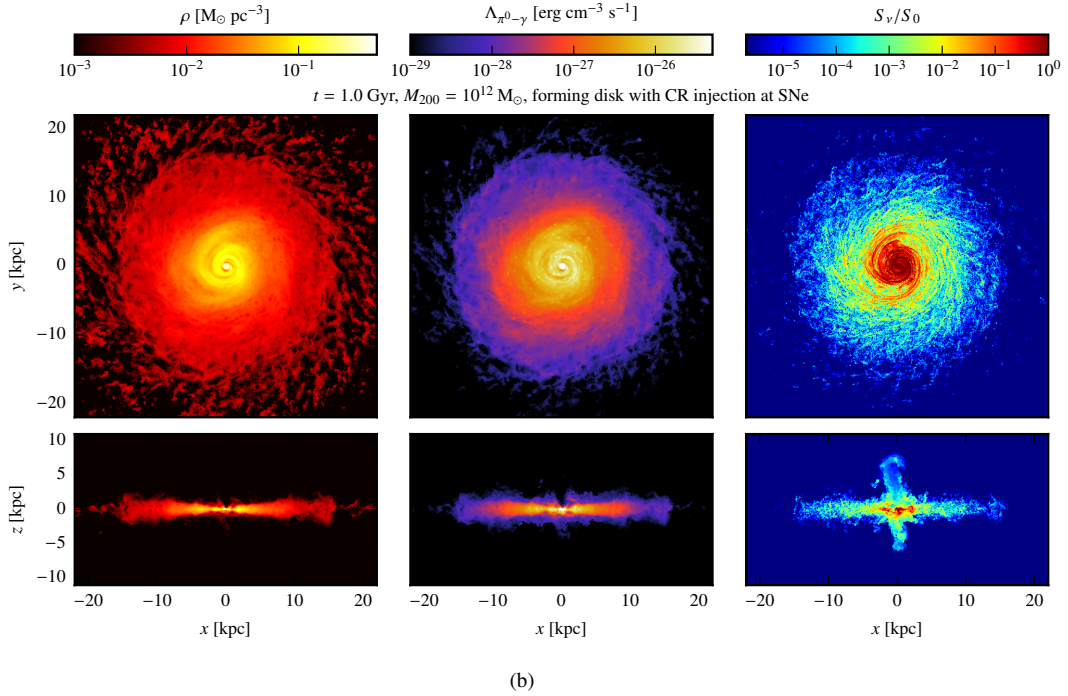
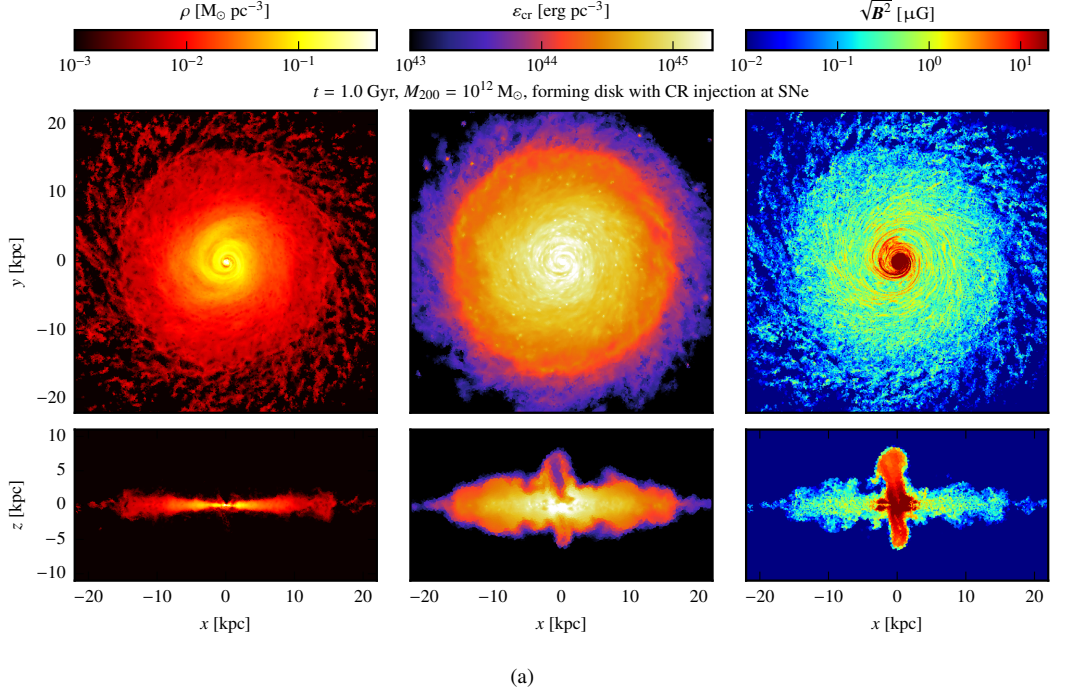


FIGURE 6. Properties of the gas disk in our $10^{12} M_{\odot}$ halo after 1 Gyrs for the anisotropic CR diffusion model. We show cross-sections of gas properties in the mid-plane of the disk (face-on views) and vertical cut-planes through the center (edge-on views) of the gas density (left panels), CR energy density (middle panels, a), and the magnetic field strength (right panels, a). The starburst-driven bubble-shaped outflows is not present in the slice showing the pion decay γ -ray emissivity above 100 MeV (middle panels, b) and visible as a weak emission feature in the secondary radio synchrotron emission at 1.4 GHz (right panels, b).

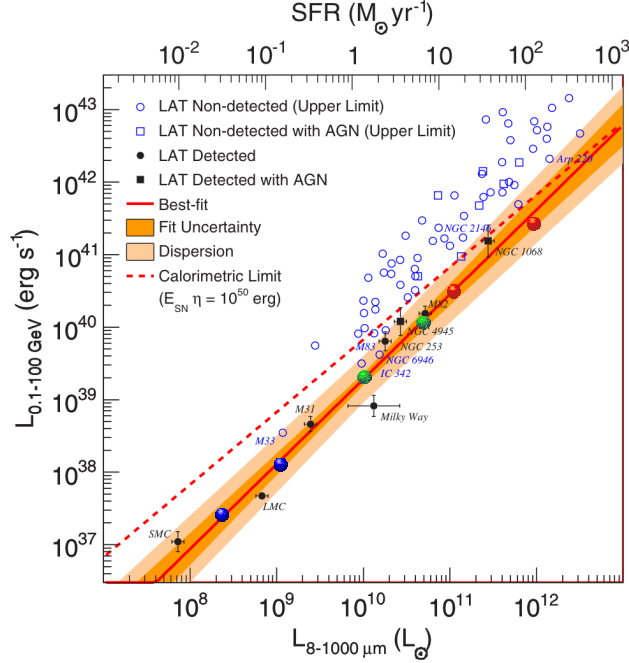


FIGURE 7. Far-infrared γ -ray correlation (adapted from [61] and enhanced by our simulation data). We color code the γ -ray emission of our simulation models for different halo masses with 10^{10} , 10^{11} , and $10^{12} M_{\odot}$ (blue, green, red) at the peak of the starburst and at 1 Gyr, respectively.

In order to explore the role of non-thermal emission in understanding galactic outflows, we run a Milky-Way-mass galaxy ($10^{12} M_{\odot}$ halo) with anisotropic CR diffusion. The disk formation generates a powerful initial starburst that injects and accumulates CRs in the center of the disk. After 0.5 Gyrs, the predominantly toroidal field configuration is reorienting in the center, potentially via a CR-driven Parker instability. This enables CRs to diffuse vertically and to lead the gas. Once the CR pressure gradient dominates the force balance, a powerful outflow is launched that plows through the halo gas. After 1 Gyr its morphology resembles the bubble-shaped γ -ray emission structure in our Milky Way (Fig. 6 a). The internal pressure in the bubble regions is dominated by CR and magnetic pressure, but remains fairly underdense. Thus, the bubble region has a negligible pion-decay γ -ray emission signature because of the depletion of target gas, dwarfing even the outskirts of the disk (Fig. 6 b). This is consistent with an unbiased, non-parametric analysis of the *Fermi* γ -ray sky [62]. Assuming a steady-state between the injection of secondaries and radiative cooling, enables to predict the resulting secondary synchrotron emission. Unlike the pion-decay γ -ray emission, the bubble contours are weakly visible in the secondary radio emission, delineating the poloidally draped magnetic field component.

The currently favored picture of galaxy formation proposes that the star formation rate correlates with the abundance of supernova remnants, which ensue proton acceleration and pion-decay γ -rays that are induced by CRp-p interactions. In the Milky Way, the pion-decay γ -ray emission dominates the total GeV γ -ray luminosity. Starburst regions are characterized by dense material with average densities of $\langle n \rangle \sim 250 \text{ cm}^{-3}$ so that the hadronic loss time scale approaches the diffusive escape time, which implies that those systems are approaching the calorimetric limit. The tight correlation of the far-infra-red (IR) and radio emission implies a universal conversion of star formation to CR electron acceleration to radio synchrotron emission. Recently, there has been an analogous relation discovered, the far-IR – γ -ray correlation (see Fig. 7, adapted from [61]). In order to connect our simulation models to these observations, we integrate the simulated pion-decay γ -ray emission between 100 MeV and 100 GeV in simulations of different halo masses with 10^{10} , 10^{11} , and $10^{12} M_{\odot}$, each at the peak of the starburst phase and after 1 Gyr. Figure 7 shows that our three-dimensional MHD-CR simulations can reproduce the slope of the observed mean relation, supporting the current picture. However, these simulations assumed a universal diffusion coefficient of $10^{28} \text{ cm}^2 \text{ s}^{-1}$ parallel to the magnetic field, which is hardly an appropriate description across a wide range of halo masses and star formation rates. Future research will show whether a similar conclusion holds for the more general case of CR streaming [63].

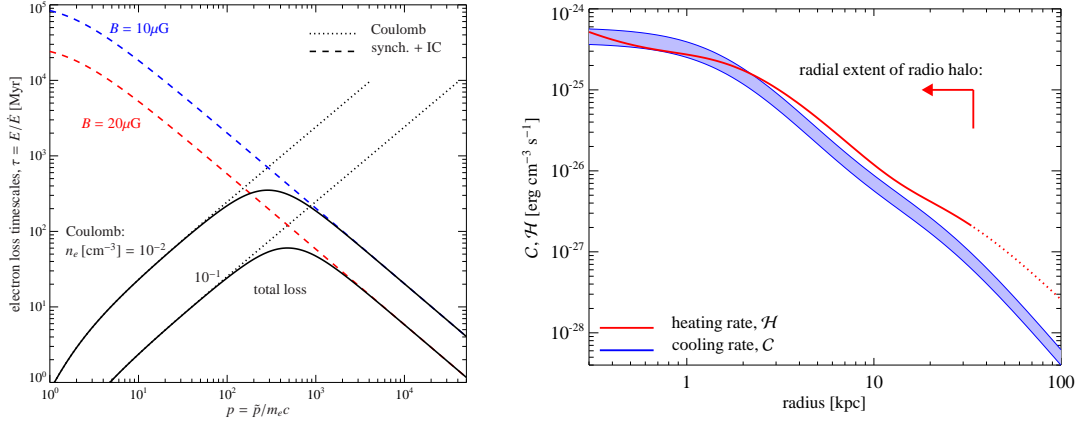


FIGURE 8. *Left.* Cooling time of electrons for conditions in the central region of the Virgo galaxy cluster as a function of normalized electron momentum, where \tilde{p} is the physical momentum. During their advective transport in the radio lobe, the (high-energy) electrons experience IC and synchrotron losses. After the electrons mix with the ambient thermal plasma, Coulomb interactions can thermalize them. Electrons with kinetic energy $E \simeq p m_e c^2 \simeq 150$ MeV are the most long-lived, with a maximum cooling time of $\tau \simeq 40$ Myr that corresponds to the radio halo age. *Right.* Cooling vs. heating rates in Virgo as a function of cluster-centric radius. The radiative cooling rates (blue) are globally balanced at each radius by streaming CRs that excited the Alfvén wave instability (red), suggesting a physical solution to the ‘cooling flow problem’ (adapted from [51]).

FEEDBACK BY ACTIVE GALACTIC NUCLEI

Galaxy clusters are the largest gravitationally-collapsed objects in the universe that have most recently formed in cosmic history. Most of the ordinary matter in clusters is composed of hot gas that emits in X-rays, thereby cooling the gas. Cooling gas becomes denser, increasing the cooling rate furthermore. This is a run-away process, which should form stars at rates up to several hundred $M_\odot \text{ yr}^{-1}$ [64] and cold gas at the cluster centers. However, the predicted amount of cold material has not been observed, constituting the famous ‘cooling flow problem’. Over the last decades, it has become clear that cluster centers host super-massive black holes with masses exceeding billions of solar masses. When a small amount of gas cools, it falls to the center and accretes onto the super-massive black hole. A fraction of it gets ejected in powerful outflows of very energetic particles (electrons and protons). Those push the ambient, X-ray emitting gas away to create spectacular, radio-emitting lobes – potentially representing the signposts of a self-regulated feedback loop. While the total available energy in these lobes is more than enough to offset the cooling, it is far from clear whether this is the long-sought solution to the ‘cooling flow problem’ and if so, how this heating process exactly works [65]. Moreover, the gas shows a central temperature floor, which previously suggested models have failed to explain.

New observations of non-thermal particle populations in the central galaxy M87 of the Virgo galaxy cluster enable us to put forward a comprehensive model for the physical heating mechanism of this long-standing problem. Low-frequency radio emission traces out an aged population of energetic electrons, thus enabling a glimpse at the distant past of the feedback cycle. However, observations by the LOw-Frequency ARray (LOFAR) revealed the absence of fossil CR electrons in the radio halo surrounding the center of the Virgo cluster [66]. This puzzle can be resolved by accounting for the release of these energetic electrons from the radio lobes and the subsequent mixing with the dense ambient intracluster gas. As a result, the energetic electrons thermalize on a timescale similar to the radio halo age of 40 million years, hiding an aged electron population from LOFAR (see left panel of Fig. 8). However, this picture also implies the release of CR protons from the lobes that will inevitably interact hadronically with the ambient gas to produce an observable γ -ray signal. Interestingly, such a signal has been detected towards Virgo with the γ -ray observatories Fermi and H.E.S.S. [67]. While the high state is time variable and possibly associated with the jet, the low state of the emission shows spectral characteristics that match our expectations from the radio results, enabling us to infer the pressure of CRs that are responsible for the observed γ -ray signal [51].

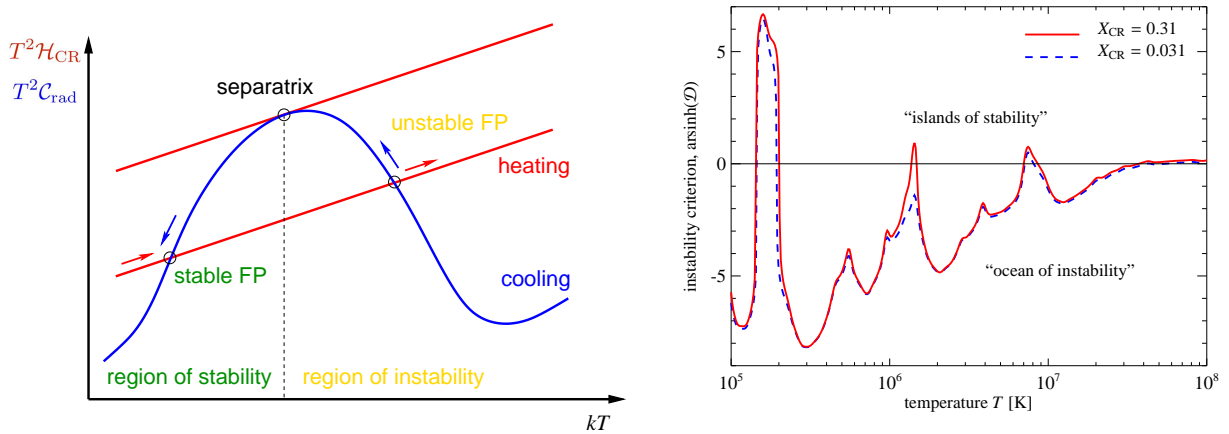


FIGURE 9. Local stability analysis of a fluid for which CR heating globally balances radiative cooling by bremsstrahlung and line emission (assuming solar metallicity). *Left.* Schematic diagram showing the importance of local temperature derivatives of the heating and cooling rates (red and blue) at fixed points of global heating-cooling balance. The equality of the temperature derivatives defines a separatrix that divides the region of stability from the region of instability. *Right.* We show the instability criterion, \mathcal{D} , as a function of temperature for parameters appropriate for M87 (red) and for a 10 times lower CR pressure (blue dashed). Once the gas temperature drops below 3×10^7 K, it becomes thermally unstable. Assuming that the gas cools while maintaining thermal equilibrium, its collapse is halted at around 10^7 K by the first ‘island of stability’, which is consistent with the temperature floor seen in X-ray observations. However, the high-density tail of density fluctuations should be able to cross this island and become again subject to thermal instability, likely sourcing some of the observable multi-phase gas (adapted from [51]).

Those CR protons are tied to magnetic fields and to excite Alfvén waves through the streaming instability. Non-linear Landau damping of those waves heats the surrounding thermal plasma at a rate that scales with the amount of energetic protons. It turns out that the amount of energetic protons required to explain the γ -ray emission yields a heating rate that balances that of radiative cooling on average at each radius (see right panel of Fig. 8 and [51]). However, the resulting global thermal equilibrium of the hot ICM is locally unstable and allows for the formation of the observed multi-phase medium through thermal instability. Provided that this heating process balances cooling during the emerging ‘cooling flow’, CR heating is locally stabilized at $kT \sim 1$ keV, causing the collapse of the majority of the gas to be halted at the observed temperature floor (see Fig. 9). We show that both the existence of a temperature floor and the similar radial scaling of the heating and cooling rates are generic results of the described heating model [52, 53]. This model makes several predictions that will be tested with future observations. If successful, this will have profound implications for our understanding of the evolution of galaxy clusters and the star formation in the central cluster galaxies. In conclusion, this paper highlights the importance of the γ -ray window and deep CTA observations for understanding the physics of galaxy formation and galaxy cluster evolution.

ACKNOWLEDGMENTS

We acknowledge support by the European Research Council under ERC-CoG grant CRAGSMAN-646955, ERC-StG grant EXAGAL-308037 and by the Klaus Tschira Foundation. VS and KS acknowledge support through subproject EXAMAG of the Priority Program 1648 ‘Software for Exascale Computing’ of the German Science Foundation.

REFERENCES

- [1] S. D. M. White and M. J. Rees, *MNRAS* **183**, 341–358 (1978).
- [2] M. J. Rees and J. P. Ostriker, *MNRAS* **179**, 541–559 (1977).

- [3] B. P. Moster, R. S. Somerville, and C. Maulbetsch et al., *ApJ* **710**, 903–923 (2010).
- [4] J. Schaye, C. Dalla Vecchia, and C. M. Booth et al., *MNRAS* **402**, 1536–1560 (2010).
- [5] J. Guedes, S. Callegari, P. Madau, and L. Mayer, *ApJ* **742**, p. 76 (2011).
- [6] E. Puchwein and V. Springel, *MNRAS* **428**, 2966–2979 (2013).
- [7] P. F. Hopkins, D. Kereš, and J. Oñorbe et al., *MNRAS* **445**, 581–603 (2014).
- [8] F. Marinacci, R. Pakmor, and V. Springel, *MNRAS* **437**, 1750–1775 (2014).
- [9] B. M. B. Henriques, S. D. M. White, and P. A. Thomas et al., *MNRAS* 2663–2680 (2015).
- [10] M. Vogelsberger, S. Genel, and V. Springel et al., *MNRAS* **444**, 1518–1547 (2014).
- [11] J. Schaye, R. A. Crain, and R. G. Bower et al., *MNRAS* **446**, 521–554 (2015).
- [12] V. Springel and L. Hernquist, **339**, 289–311 (2003).
- [13] J. Schaye and C. Dalla Vecchia, *MNRAS* **383**, 1210–1222 (2008).
- [14] B. D. Oppenheimer and R. Davé, *MNRAS* **373**, 1265–1292 (2006).
- [15] T. Di Matteo, V. Springel, and L. Hernquist, *Nature* **433**, 604–607 (2005).
- [16] V. Springel, T. Di Matteo, and L. Hernquist, *MNRAS* **361**, 776–794 (2005).
- [17] R. B. Larson, *MNRAS* **169**, 229–246 (1974).
- [18] A. Dekel and J. Silk, *ApJ* **303**, 39–55 (1986).
- [19] D. Ceverino and A. Klypin, *ApJ* **695**, 292–309 (2009).
- [20] N. Murray, E. Quataert, and T. A. Thompson, *ApJ* **618**, 569–585 (2005).
- [21] T. A. Thompson, E. Quataert, and N. Murray, *ApJ* **630**, 167–185 (2005).
- [22] M. R. Krumholz and T. A. Thompson, *ApJ* **760**, p. 155 (2012).
- [23] J. Rosdahl, J. Schaye, R. Teyssier, and O. Agertz, *MNRAS* **451**, 34–58 (2015).
- [24] M. A. Skinner and E. C. Ostriker, *ApJ* **809**, p. 187 (2015).
- [25] A. Boulares and D. P. Cox, *ApJ* **365**, 544–558 (1990).
- [26] F. M. Ipavich, *ApJ* **196**, 107–120 (1975).
- [27] D. Breitschwerdt, J. F. McKenzie, and H. J. Voelk, *A&A* **245**, 79–98 (1991).
- [28] V. N. Zirakashvili, D. Breitschwerdt, V. S. Ptuskin, and H. J. Voelk, *A&A* **311**, 113–126 (1996).
- [29] V. S. Ptuskin, H. J. Voelk, V. N. Zirakashvili, and D. Breitschwerdt, *A&A* **321**, 434–443 (1997).
- [30] D. Breitschwerdt, V. A. Dogiel, and H. J. Völk, *A&A* **385**, 216–238 (2002).
- [31] A. Socrates, S. W. Davis, and E. Ramirez-Ruiz, *ApJ* **687**, 202–215 (2008).
- [32] J. E. Everett, E. G. Zweibel, and R. A. Benjamin et al., *ApJ* **674**, 258–270 (2008).
- [33] J. E. Everett, Q. G. Schiller, and E. G. Zweibel, *ApJ* **711**, 13–24 (2010).
- [34] S. Samui, K. Subramanian, and R. Srianand, *MNRAS* **402**, 2778–2791 (2010).
- [35] E. A. Dorfi and D. Breitschwerdt, *A&A* **540**, p. A77 (2012).
- [36] M. Hanasz, H. Lesch, and T. Naab et al., *ApJ* **777**, p. L38 (2013).
- [37] P. Girichidis, T. Naab, and S. Walch et al., *ApJ* **816**, p. L19 (2016).
- [38] C. M. Simpson, R. Pakmor, and F. Marinacci et al., *ApJ* **827**, p. L29 (2016).
- [39] R. Tüllmann, R.-J. Dettmar, M. Soida, M. Urbanik, and J. Rossa, *A&A* **364**, L36–L41 (2000).
- [40] L. F. S. Rodrigues, G. R. Sarson, A. Shukurov, P. J. Bushby, and A. Fletcher, *ApJ* **816**, p. 2 (2016).
- [41] M. Uhlig, C. Pfrommer, and M. Sharma et al., *MNRAS* **423**, 2374–2396 (2012).
- [42] M. Ruzkowski, H.-Y. K. Yang, and E. Zweibel, (2016), arXiv:1602.04856 .
- [43] C. M. Booth, O. Agertz, A. V. Kravtsov, and N. Y. Gnedin, *ApJ* **777**, p. L16 (2013).
- [44] M. Salem and G. L. Bryan, *MNRAS* **437**, 3312–3330 (2014).
- [45] M. Salem, G. L. Bryan, and C. Hummels, *ApJ* **797**, p. L18 (2014).
- [46] M. Loewenstein, E. G. Zweibel, and M. C. Begelman, *ApJ* **377**, 392–402 (1991).
- [47] F. Guo and S. P. Oh, *MNRAS* 251–266 (2008).
- [48] T. Enßlin, C. Pfrommer, F. Miniati, and K. Subramanian, *A&A* **527**, p. A99 (2011).
- [49] Y. Fujita and Y. Ohira, *ApJ* **746**, p. 53 (2012).
- [50] J. Wiener, S. P. Oh, and F. Guo, *MNRAS* **434**, 2209–2228 (2013).
- [51] C. Pfrommer, *ApJ* **779**, p. 10 (2013).
- [52] S. Jacob and C. Pfrommer, (2016), arXiv:1609.06321 .
- [53] S. Jacob and C. Pfrommer, (2016), arXiv:1609.06322 .
- [54] V. Springel, *MNRAS* **401**, 791–851 (2010).
- [55] R. Pakmor, A. Bauer, and V. Springel, *MNRAS* **418**, 1392–1401 (2011).
- [56] R. Blandford and D. Eichler, *Phys. Rep.* **154**, 1–75 (1987).
- [57] C. Pfrommer, R. Pakmor, K. Schaal, C. M. Simpson, and V. Springel, (2016), arXiv:1604.07399 .
- [58] R. Pakmor, C. Pfrommer, C. M. Simpson, R. Kannan, and V. Springel, *MNRAS* **462**, 2603–2616 (2016).
- [59] R. Kulsrud and W. P. Pearce, *ApJ* **156**, p. 445 (1969).
- [60] R. Pakmor, C. Pfrommer, C. M. Simpson, and V. Springel, *ApJ* **824**, p. L30 (2016).
- [61] M. Ackermann, M. Ajello, and A. Allafort et al., *ApJ* **755**, p. 164 (2012).
- [62] M. Selig, V. Vacca, N. Oppermann, and T. A. Enßlin, *A&A* **581**, p. A126 (2015).
- [63] J. Wiener, C. Pfrommer, and S. P. Oh, (2016), arXiv:1608.02585 .
- [64] J. R. Peterson and A. C. Fabian, *Phys. Rep.* **427**, 1–39 (2006).
- [65] B. R. McNamara and P. E. J. Nulsen, *ARA&A* **45**, 117–175 (2007).
- [66] F. de Gasperin, E. Orrú, and M. Murgia et al., *A&A* **547**, p. A56 (2012).
- [67] F. M. Rieger and F. Aharonian, *Modern Physics Letters A* **27**, p. 30030 (2012).